YITP-SB-11-11

SUSY QCD corrections to Higgs-b Production: Is the Δ_b Approximation Accurate?

S. Dawson[a], C. B. Jackson[b], P. Jaiswal[a,c]

[a] *Department of Physics, Brookhaven National Laboratory, Upton, NY 11973, USA*

[b] *Physics Department, University of Texas, Arlington, Texas*

[c] *Yang Institute for Theoretical Physics, Stony Brook University, Stony Brook, NY 11790, USA*

arXiv:1104.1631v2 [hep-ph] 19 May 2011

Abstract

The associated production of a Higgs boson with a b quark is a discovery channel for the lightest MSSM neutral Higgs boson. We consider the SUSY QCD contributions from squarks and gluinos and discuss the decoupling properties of these effects. A detailed comparison of our exact $\mathcal{O}(\alpha_s)$ results with those of a widely used effective Lagrangian approach, the Δ_b approximation, is presented. The Δ_b approximation is shown to accurately reproduce the exact one-loop SQCD result to within a few percent over a wide range of parameter space.

I. INTRODUCTION

Once a light Higgs-like particle is discovered it will be critical to determine if it is the Higgs Boson predicted by the Standard Model. The minimal supersymmetric Standard Model (MSSM) presents a comparison framework in which to examine the properties of a putative Higgs candidate. The MSSM Higgs sector contains 5 Higgs bosons–2 neutral bosons, h and H, a pseudoscalar boson, A, and 2 charged bosons, $H^{\pm}$. At the tree level the theory is described by just 2 parameters, which are conveniently chosen to be M_A, the mass of the pseudoscalar boson, and $\tan\beta$, the ratio of vacuum expectation values of the 2 neutral Higgs bosons. Even when radiative corrections are included, the theory is highly predictive[1–3].

In the MSSM, the production mechanisms for the Higgs bosons can be significantly different from in the Standard Model. For large values of $\tan\beta$, the heavier Higgs bosons, A and H, are predominantly produced in association with b quarks. Even for $\tan\beta \sim 5$, the production rate in association with b quarks is similar to that from gluon fusion for A and H production[19]. For the lighter Higgs boson, h, for $\tan\beta \gtrsim 7$ the dominant production mechanism at both the Tevatron and the LHC is production with b quarks for light M_A ($\lesssim 200\ GeV$), where the $b\overline{b}h$ coupling is enhanced . Both the Tevatron[4] and the LHC experiments[5] have presented limits Higgs production in association with b quarks, searching for the decays $h \to \tau^+\tau^-$ and $b\overline{b}$[1]. These limits are obtained in the context of the MSSM are sensitive to the b-squark and gluino loop corrections which we consider here.

The rates for bh associated production at the LHC and the Tevatron have been extensively studied[8–18] and the NLO QCD correction are well understood, both in the 4- and 5-flavor number parton schemes[9, 11, 15]. In the 4- flavor number scheme, the lowest order processes for producing a Higgs boson and a b quark are $gg \to b\overline{b}h$ and $q\overline{q} \to b\overline{b}h$[8, 12, 17]. In the 5− flavor number scheme, the lowest order process is $bg \to bh$ ($\overline{b}g \to \overline{b}h$). The two schemes represent different orderings of perturbation theory and calculations in the two schemes produce rates which are in qualitative agreement[11, 19]. In this paper, we use the 5-flavor number scheme for simplicity. The resummation of threshold logarithms[20], electroweak corrections[21, 22] and SUSY QCD corrections[23] have also been computed for

[1] The expected sensitivities of ATLAS and CMS to b Higgs associated production are described in Refs. [6, 7].

bh production in the 5− flavor number scheme.

Here, we focus on the role of squark and gluino loops. The properties of the SUSY QCD corrections to the $b\overline{b}h$ vertex, both for the decay $h \to b\overline{b}$[24–27] and the production, $b\overline{b} \to h$[12, 27–29], were computed long ago. The contributions from b squarks and gluinos to the lightest MSSM Higgs boson mass are known at 2-loops[30, 31], while the 2-loop SQCD contributions to the $b\overline{b}h$ vertex is known in the limit in which the Higgs mass is much smaller than the squark and gluino masses[32, 33]. The contributions of squarks and gluinos to the on-shell $b\overline{b}h$ vertex are non-decoupling for heavy squark and gluino masses and decoupling is only achieved when the pseudoscalar mass, M_A, also becomes large.

An effective Lagrangian approach, the Δ_b approximation[25, 26], can be used to approximate the SQCD contributions to the on-shell $b\overline{b}h$ vertex and to resum the $(\alpha_s \tan\beta/M_{SUSY})^n$ enhanced terms. The numerical accuracy of the Δ_b effective Lagrangian approach has been examined for a number of cases. The 2−loop contributions to the lightest MSSM Higgs boson mass of $\mathcal{O}(\alpha_b\alpha_s)$ were computed in Refs. [30] and [31], and it was found that the majority of these corrections could be absorbed into a 1−loop contribution by defining an effective b quark mass using the Δ_b approach. The sub-leading contributions to the Higgs boson mass (those not absorbed into Δ_b) are then of $\mathcal{O}(1\ GeV)$. The Δ_b approach also yields an excellent approximation to the SQCD corrections for the decay process $h \to b\overline{b}$[27]. It is particularly interesting to study the accuracy of the Δ_b approximation for production processes where one of the b quarks is off-shell. The SQCD contributions from squarks and gluinos to the inclusive Higgs production rate in association with b quarks has been studied extensively in the 4FNS in Ref. [37], where the the lowest order contribution is $gg \to b\overline{b}h$. In the 4FNS, the inclusive cross section including the exact 1-loop SQCD corrections is reproduced to within a few percent using the Δ_b approximation. However, the accuracy of the Δ_b approximation for the MSSM neutral Higgs boson production in the 5FNS has been studied for only a small set of MSSM parameters in Ref. [23]. The major new result of this paper is a detailed study of the accuracy of the Δ_b approach in the 5FNS for the $bg \to bh$ production process. In this case, one of the b quarks is off-shell and there are contributions which are not contained in the effective Lagrangian approach.

The plan of the paper is as follows: Section 2 contains a brief review of the MSSM Higgs and b squark sectors and also a review of the effective Lagrangian approximation. The calculation of Ref. [23] is summarized in Section 2. We include SQCD contributions to

bh production which are enhanced by $m_b \tan\beta$ which were omitted in Ref. [23]. Analytic results for the SQCD corrections to $bg \to bh$ in the extreme mixing scenarios in the b squark sector are presented in Section 3. Section 4 contains numerical results for the $\sqrt{s} = 7$ TeV LHC. Finally, our conclusions are summarized in Section 5. Detailed analytic results are relegated to a series of appendices.

II. BASICS

A. MSSM Framework

In the simplest version of the MSSM there are two Higgs doublets, H_u and H_d, which break the electroweak symmetry and give masses to the W and Z gauge bosons. The neutral Higgs boson masses are given at tree level by,

$$M^2_{h,H} = \frac{1}{2}\left[M^2_A + M^2_Z \mp \sqrt{(M^2_A + M^2_Z)^2 - 4M^2_A M^2_Z \cos^2 2\beta}\right], \tag{1}$$

and the angle, α, which diagonalizes the neutral Higgs mass is

$$\tan 2\alpha = \tan 2\beta \left(\frac{M^2_A + M^2_Z}{M^2_A - M^2_Z}\right). \tag{2}$$

In practice, the relations of Eqs. 1 and 2 receive large radiative corrections which must be taken into account in numerical studies. We use the program FeynHiggs[34–36] to generate the Higgs masses and an effective mixing angle, α_{eff}, which incorporates higher order effects.

The scalar partners of the left- and right- handed b quarks, $\tilde{b}_L$ and $\tilde{b}_R$, are not mass eigenstates, but mix according to,

$$L_M = -(\tilde{b}^*_L, \tilde{b}^*_R) M^2_{\tilde{b}} \begin{pmatrix} \tilde{b}_L \\ \tilde{b}_R \end{pmatrix}. \tag{3}$$

The $\tilde{b}$ squark mass matrix is,

$$M^2_{\tilde{b}} = \begin{pmatrix} \tilde{m}^2_L & m_b X_b \\ m_b X_b & \tilde{m}^2_R \end{pmatrix}, \tag{4}$$

and we define,

$$\begin{aligned} X_b &= A_b - \mu \tan\beta \\ \tilde{m}^2_L &= M^2_Q + m^2_b + M^2_Z \cos 2\beta (I^b_3 - Q_b \sin^2\theta_W) \\ \tilde{m}^2_R &= M^2_D + m^2_b + M^2_Z \cos 2\beta Q_b \sin^2\theta_W . \end{aligned} \tag{5}$$

$M_{Q,D}$ are the soft SUSY breaking masses, $I_3^b = -1/2$, and $Q_b = -1/3$. The parameter A_b is the trilinear scalar coupling of the soft supersymmetry breaking Lagrangian and μ is the Higgsino mass parameter. The b squark mass eigenstates are $\tilde{b}_1$ and $\tilde{b}_2$ and define the b-squark mixing angle, $\tilde{\theta}_b$

$$\begin{aligned} \tilde{b}_1 &= \cos\tilde{\theta}_b\tilde{b}_L + \sin\tilde{\theta}_b\tilde{b}_R \\ \tilde{b}_2 &= -\sin\tilde{\theta}_b\tilde{b}_L + \cos\tilde{\theta}_b\tilde{b}_R \,. \end{aligned} \tag{6}$$

At tree level,

$$\sin 2\tilde{\theta}_b = \frac{2m_b(A_b - \mu\tan\beta)}{M^2_{\tilde{b}_1} - M^2_{\tilde{b}_2}} \tag{7}$$

and the sbottom mass eigenstates are,

$$M^2_{\tilde{b}_1,\tilde{b}_2} = \frac{1}{2}\left[\tilde{m}_L^2 + \tilde{m}_R^2 \mp \sqrt{(\tilde{m}_L^2 - \tilde{m}_R^2)^2 + 4m_b^2X_b^2}\right]. \tag{8}$$

B. Δ_b Approximation: The Effective Lagrangian Approach

Loop corrections which are enhanced by powers of $\alpha_s\tan\beta$ can be included in an effective Lagrangian approach. At tree level, there is no $\overline{\psi}_L b_R H_u$ coupling in the MSSM, but such a coupling arises at one loop and gives an effective interaction[25–27][2],

$$L_{eff} = -\lambda_b\overline{\psi}_L\left(H_d + \frac{\Delta_b}{\tan\beta}H_u\right)b_R + h.c. \quad . \tag{9}$$

Eq. 9 shifts the b quark mass from its tree level value, [3]

$$m_b \to \frac{\lambda_b v_1}{\sqrt{2}}(1+\Delta_b)\,, \tag{10}$$

and also implies that the Yukawa couplings of the Higgs bosons to the b quark are shifted from the tree level predictions. This shift of the Yukawa couplings can be included with an effective Lagrangian approach[26, 27],

$$L_{eff} = -\frac{m_b}{v_{SM}}\left(\frac{1}{1+\Delta_b}\right)\left(-\frac{\sin\alpha}{\cos\beta}\right)\left(1 - \frac{\Delta_b}{\tan\beta\tan\alpha}\right)\overline{b}bh\,. \tag{11}$$

The Lagrangian of Eq. 11 has been shown to sum all terms of $\mathcal{O}(\alpha_s\tan\beta)^n$ for large $\tan\beta$[25, 26].[4] This effective Lagrangian has been used to compute the SQCD corrections

[2] The neutral components of the Higgs bosons receive vacuum expectation values: $\langle H_d^0\rangle = \frac{v_1}{\sqrt{2}}, \langle H_u^0\rangle = \frac{v_2}{\sqrt{2}}$.
[3] $v_{SM} = (\sqrt{2}G_F)^{-1/2}$, $v_1 = v_{SM}\cos\beta$
[4] It is also possible to sum the contributions which are proportional to A_b, but these terms are less important numerically[27].

to both the inclusive production process, $b\overline{b} \to h$, and the decay process, $h \to b\overline{b}$, and yields results which are within a few percent of the exact one-loop SQCD calculations[27, 37].

The expression for Δ_b is found in the limit $m_b << M_h, M_Z << M_{\tilde{b}_1}, M_{\tilde{b}_2}, M_{\tilde{g}}$. The 1-loop contribution to Δ_b from sbottom/gluino loops is[25, 26, 38]

$$\Delta_b = \frac{2\alpha_s(\mu_S)}{3\pi} M_{\tilde{g}} \mu \tan\beta I(M_{\tilde{b_1}}, M_{\tilde{b_2}}, M_{\tilde{g}}) \,, \tag{12}$$

where the function $I(a,b,c)$ is,

$$I(a,b,c) = \frac{1}{(a^2-b^2)(b^2-c^2)(a^2-c^2)} \left\{ a^2 b^2 \log\left(\frac{a^2}{b^2}\right) + b^2 c^2 \log\left(\frac{b^2}{c^2}\right) + c^2 a^2 \log\left(\frac{c^2}{a^2}\right) \right\}, \tag{13}$$

and $\alpha_s(\mu_S)$ should be evaluated at a typical squark or gluino mass. The 2−loop QCD corrections to Δ_b have been computed and demonstrate that the appropriate scale at which to evaluate Δ_b is indeed of the order of the heavy squark and gluino masses[32, 33]. The renormalization scale dependence of Δ_b is minimal around $\mu_0/3$, where $\mu_0 \equiv (M_{\tilde{g}} + m_{\tilde{b}_1} + m_{\tilde{b}_2})/3$. In our language this is a high scale, of order the heavy SUSY particle masses. The squarks and gluinos are integrated out of the theory at this high scale and their effects contained in Δ_b. The effective Lagrangian is then used to calculate light Higgs production at a low scale, which is typically the electroweak scale, $\sim 100\ GeV$.

Using the effective Lagrangian of Eq. 9, which we term the Improved Born Approximation (or Δ_b approximation), the cross section is written in terms of the effective coupling,

$$g_{bbh}^{\Delta_b} \equiv g_{bbh} \left(\frac{1}{1+\Delta_b}\right)\left(1 - \frac{\Delta_b}{\tan\beta \tan\alpha}\right), \tag{14}$$

where

$$g_{bbh} = -\left(\frac{\sin\alpha}{\cos\beta}\right) \frac{\overline{m}_b(\mu_R)}{v_{SM}} \,. \tag{15}$$

We evaluate $\overline{m_b}(\mu_R)$ using the 2−loop $\overline{MS}$ value at a scale μ_R of $\mathcal{O}(M_h)$, and use the value of α_{eff} determined from FeynHiggs. The Improved Born Approximation consists of rescaling the tree level cross section, σ_0, by the coupling of Eq. 14[5],

$$\sigma_{IBA} = \left(\frac{g_{bbh}^{\Delta_b}}{g_{bbh}}\right)^2 \sigma_0 \,. \tag{16}$$

The Improved Born Approximation has been shown to accurately reproduce the full SQCD calculation of $pp \to \overline{t}bH^+$[39, 40].

[5] This is the approximation used in Ref. [19] to include the SQCD corrections.

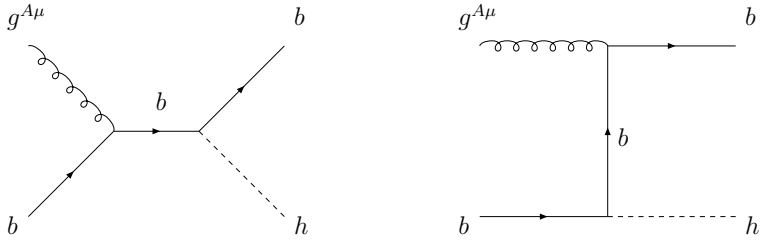


FIG. 1: Feynman diagrams for $g(q_1) + b(q_2) \to b(p_b) + h(p_h)$.

The one-loop result including the SQCD corrections for $bg \to bh$ can be written as,

$$\sigma_{SQCD} \equiv \sigma_{IBA}\Big(1 + \Delta_{SQCD}\Big), \tag{17}$$

where Δ_{SQCD} is found from the exact SQCD calculation summarized in Appendix B.

The Improved Born Approximation involves making the replacement in the tree level Lagrangian,

$$m_b \to \frac{m_b}{1 + \Delta_b}\,. \tag{18}$$

Consistency requires that this substitution also be made in the squark mass matrix of Eq. 4[41, 42]

$$M^2_{\tilde{b}} \to \begin{pmatrix} \tilde{m}^2_L & \left(\frac{m_b}{1+\Delta_b}\right) X_b \\ \left(\frac{m_b}{1+\Delta_b}\right) X_b & \tilde{m}^2_R \end{pmatrix}. \tag{19}$$

The effects of the substitution of Eq. 18 in the b-squark mass matrix are numerically important, although they generate contributions which are formally higher order in α_s. Eqs. 12 and 19 can be solved iteratively for $M_{\tilde{b}_1}$, $M_{\tilde{b}_2}$ and Δ_b using the proceedure of Ref. [41][6].

C. SQCD Contributions to $gb \to bh$

The contributions from squark and gluino loops to the $gb \to bh$ process have been computed in Ref. [23] in the $m_b = 0$ limit. We extend that calculation by including terms which are enhanced by $m_b \tan\beta$ and provide analytic results in several useful limits.

The tree level diagrams for $g(q_1) + b(q_2) \to b(p_b) + h(p_h)$ are shown in Fig. 1. We define

[6] We use FeynHiggs only for calculating M_h and $\sin\alpha_{eff}$.

the following dimensionless spinor products

$$\begin{aligned}
M_s^\mu &= \frac{\overline{u}\left(p_b\right)\left(\not{q}_1+\not{q}_2\right)\gamma^\mu u\left(q_2\right)}{s} \\
M_t^\mu &= \frac{\overline{u}\left(p_b\right)\gamma^\mu\left(\not{p}_b-\not{q}_1\right)u\left(q_2\right)}{t} \\
M_1^\mu &= q_2^\mu\frac{\overline{u}\left(p_b\right)u\left(q_2\right)}{u} \\
M_2^\mu &= \frac{\overline{u}\left(p_b\right)\gamma^\mu u\left(q_2\right)}{m_b} \\
M_3^\mu &= p_b^\mu\frac{\overline{u}\left(p_b\right)\not{q}_1 u\left(q_2\right)}{m_b t} \\
M_4^\mu &= q_2^\mu\frac{\overline{u}\left(p_b\right)\not{q}_1 u\left(q_2\right)}{m_b s}\,,
\end{aligned} \tag{20}$$

where $s=(q_1+q_2)^2, t=(p_b-q_1)^2$ and $u=(p_b-q_2)^2$. In the $m_b=0$ limit, the tree level amplitude depends only on M_s^μ and M_t^μ, and M_1^μ is generated at one-loop. When the effects of the b mass are included, M_2^μ, M_3^μ, and M_4^μ are also generated.

The tree level amplitude is

$$\mathcal{A}^a_{\alpha\beta}\mid_0 \;=\; -g_s g_{bbh}\left(T^a\right)_{\alpha\beta}\epsilon_\mu(q_1)\left\{M_s^\mu+M_t^\mu\right\}\,, \tag{21}$$

and the one loop contribution can be written as

$$\mathcal{A}^a_{\alpha\beta}=-\frac{\alpha_s(\mu_R)}{4\pi}g_s g_{bbh}\left(T^a\right)_{\alpha\beta}\sum_j X_j M_j^\mu\epsilon_\mu(q_1)\,. \tag{22}$$

In the calculations to follow, only the non-zero X_j coefficients are listed and we neglect terms of $\mathcal{O}(m_b^2/s)$ if they are not enhanced by $\tan\beta$.

The renormalization of the squark and gluino contributions is performed in the on-shell scheme and has been described in Refs. [23, 32, 43]. The bottom quark self-energy is

$$\Sigma_b\left(p\right) \;=\; \not{p}\left(\Sigma_b^V(p^2)-\Sigma_b^A(p^2)\gamma_5\right)+m_b\Sigma_b^S(p^2)\,. \tag{23}$$

The b quark fields are renormalized as $b\to\sqrt{Z_b^V}b$ and $Z_b^V\equiv\sqrt{1+\delta Z_b^V}$. The contribution from the counter-terms to the self-energy is,

$$\begin{aligned}
\Sigma_b^{\rm ren}\left(p\right) &= \Sigma_b\left(p\right)+\delta\Sigma_b(p) \\
\delta\Sigma_b\left(p\right) &= \not{p}\left(\delta Z_b^V-\delta Z_b^A\gamma_5\right)-m_b\delta Z_b^V-\delta m_b\,.
\end{aligned} \tag{24}$$

Neglecting the γ_5 contribution, the renormalized self-energy is then given by

$$\Sigma_b^{\rm ren}\left(p\right) \;=\; \left(\not{p}-m_b\right)\left(\Sigma_b^V(p^2)+\delta Z_b^V\right)+m_b\left(\Sigma_b^S(p^2)+\Sigma_b^V(p^2)-\frac{\delta m_b}{m_b}\right)\,. \tag{25}$$

The on-shell renormalization condition implies

$$\Sigma_b^{\rm ren}(p)\big|_{\not p=m_b} \;=\; 0 \tag{26}$$

$$lim_{\not p\to m_b}\left(\frac{\Sigma_b^{\rm ren}(p)}{\not p - m_b}\right) \;=\; 0\,. \tag{27}$$

The mass and wavefunction counter-terms are[7]

$$\begin{aligned}
\frac{\delta m_b}{m_b} &= \left[\Sigma_b^S\left(p^2\right)+\Sigma_b^V\left(p^2\right)\right]_{p^2=m_b^2} \\
&= \frac{\alpha_s(\mu_R)}{3\pi}\sum_{i=1}^{2}\left[(-1)^i\,\frac{M_{\tilde g}}{m_b}s_{2\tilde b}B_0 - B_1\right]\left(0;M_{\tilde g}^2,M_{\tilde b_i}^2\right) \qquad (28)\\
\delta Z_b^V &= -\,\Sigma_b^V\left(p^2\right)\big|_{p^2=m_b^2} - 2m_b^2\frac{\partial}{\partial p^2}\left(\Sigma_b^V(p^2)+\Sigma_S(p^2)\right)\big|_{p^2=m_b^2} \\
&= \frac{\alpha_s(\mu_R)}{3\pi}\sum_{i=1}^{2}\left[B_1+2m_b^2B_1'-(-1)^i 2m_b M_{\tilde g}s_{2\tilde b}B_0'\right]\left(0;M_{\tilde g}^2,M_{\tilde b_i}^2\right)\,, \qquad (29)
\end{aligned}$$

where we consistently neglect the b quark mass if it is not enhanced by $\tan\beta$. The Passarino-Veltman functions $B_0\left(0;M_{\tilde g}^2,M_{\tilde b_i}^2\right)$ and $B_1\left(0;M_{\tilde g}^2,M_{\tilde b_i}^2\right)$ are defined in Appendix A. Using the tree level relationship of Eq. 7, the mass counterterm can be written as,

$$\frac{\delta m_b}{m_b} \;=\; \frac{2\alpha_s(\mu_R)}{3\pi}M_{\tilde g}A_b I(M_{\tilde b_1},M_{\tilde b_2},M_{\tilde g}) - \Delta_b - \frac{\alpha_s(\mu_R)}{3\pi}\sum_{i=1}^{2}B_1\left(0;M_{\tilde g}^2,M_{\tilde b_i}^2\right)\,. \tag{30}$$

The external gluon is renormalized as $g_\mu^A \to \sqrt{Z_3}g_\mu^A = \sqrt{1+\delta Z_3}g_\mu^A$ and the strong coupling renormalization is $g_s \to Z_g g_s$ with $\delta Z_g = -\delta Z_3/2$. We renormalize g_s using the $\overline{MS}$ scheme with the heavy squark and gluino contributions subtracted at zero momentum[44],

$$\delta Z_3 = -\frac{\alpha_s(\mu_R)}{4\pi}\left[\frac{1}{6}\Sigma_{\tilde q_i}\left(\frac{4\pi\mu_R^2}{M_{\tilde q_i}^2}\right)^{\epsilon}+2\left(\frac{4\pi\mu_R^2}{M_{\tilde g}^2}\right)^{\epsilon}\right]\frac{1}{\epsilon}\Gamma(1+\epsilon)\,. \tag{31}$$

In order to avoid overcounting the effects which are contained in $g_{bbh}^{\Delta_b}$ to $\mathcal{O}(\alpha_s)$, we need the additional counterterm,

$$\delta_{CT} = \Delta_b\left(1+\frac{1}{\tan\beta\tan\alpha}\right)\,. \tag{32}$$

The total contribution of the counterterms is,

$$\sigma_{CT} = \sigma_{IBA}\left(2\delta Z_b^V+\delta Z_3+2\delta Z_g+2\frac{\delta m_b}{m_b}+2\delta_{CT}\right) = 2\sigma_{IBA}\left(\delta Z_b^V+\frac{\delta m_b}{m_b}+\delta_{CT}\right)\,. \tag{33}$$

The $\tan\beta$ enhanced contributions from Δ_b cancel between Eqs. 30 and 32. The expressions for the contributions to the X_i, as defined in Eq. 22, are given in Appendix B for arbitrary squark and gluino masses, and separately for each $1-$ loop diagram.

[7] $s_{2\tilde b} \equiv \sin 2\tilde\theta_b$.

III. RESULTS FOR MAXIMAL AND MINIMAL MIXING IN THE b-SQUARK SECTOR

A. Maximal Mixing

The squark and gluino contributions to $bg \to bh$ can be examined analytically in several scenarios. In the first scenario,

$$\mid \tilde{m}_L^2 - \tilde{m}_R^2 \mid << \frac{m_b}{1+\Delta_b} \mid X_b \mid \; . \tag{34}$$

We expand in powers of $\frac{|\tilde{m}_L^2 - \tilde{m}_R^2|}{m_b X_b}$. In this case the sbottom masses are nearly degenerate,

$$\begin{aligned} M_S^2 &\equiv \frac{1}{2}\left[M_{\tilde{b}_1}^2 + M_{\tilde{b}_2}^2\right] \\ \mid M_{\tilde{b}_1}^2 - M_{\tilde{b}_2}^2 \mid &= \left(\frac{2m_b \mid X_b \mid}{1+\Delta_b}\right)\left(1 + \frac{(\tilde{m}_L^2 - \tilde{m}_R^2)^2(1+\Delta_b)^2}{8m_b^2 X_b^2}\right) << M_S^2 \, . \end{aligned} \tag{35}$$

This scenario is termed maximal mixing since

$$\sin 2\tilde{\theta}_b \sim 1 - \frac{(\tilde{m}_L^2 - \tilde{m}_R^2)^2(1+\Delta_b)^2}{8m_b^2 X_b^2} \, . \tag{36}$$

We expand the contributions of the exact one-loop SQCD calculation given in Appendix B in powers of $1/M_S$, keeping terms to $\mathcal{O}\left(\frac{M_{EW}^2}{M_S^2}\right)$ and assuming $M_S \sim M_{\tilde{g}} \sim \mu \sim A_b \sim \tilde{m}_L \sim \tilde{m}_R >> M_W, M_Z, M_h \sim M_{EW}$. In the expansions, we assume the large $\tan\beta$ limit and take $m_b \tan\beta \sim \mathcal{O}(M_{EW})$. This expansion has been studied in detail for the decay $h \to b\overline{b}$, with particular emphasis on the decoupling properties of the results as M_S and $M_{\tilde{g}} \to \infty$[28]. The SQCD contributions to the decay, $h \to b\overline{b}$, extracted from our results are in agreement with those of Refs. [28, 42]

The final result for maximal mixing, summing all contributions, is,

$$\begin{aligned} A_s &\equiv -g_s T^A g_{bbh} M_s^\mu \left\{1 + \frac{\alpha_s(\mu_R)}{4\pi} X_i^s\right\} \\ &= -g_s T^A g_{bbh} M_s^\mu \left\{1 + \left(\frac{\delta g_{bbh}}{g_{bbh}}\right)_{max} + \frac{\alpha_s(\mu_R)}{4\pi}\frac{s}{M_S^2}\delta\kappa_{max}\right\} \\ A_t &\equiv -g_s T^A g_{bbh} M_s^\mu \left\{1 + \frac{\alpha_s(\mu_R)}{4\pi} X_i^t\right\} \\ &= -g_s T^A g_{bbh} M_t^\mu \left\{1 + \left(\frac{\delta g_{bbh}}{g_{bbh}}\right)_{max}\right\} \\ A_1 &\equiv -g_s T^A g_{bbh} M_s^\mu \left\{1 + \frac{\alpha_s(\mu_R)}{4\pi} X_i^1\right\} \\ &= -g_s T^A g_{bbh} M_1^\mu \left(-\frac{\alpha_s(\mu_R) u}{2\pi M_S^2}\right)\delta\kappa_{max} \, . \end{aligned} \tag{37}$$

The contribution which is a rescaling of the $b\bar{b}h$ vertex is,

$$\left(\frac{\delta g_{bbh}}{g_{bbh}}\right)_{max} = \left(\frac{\delta g_{bbh}}{g_{bbh}}\right)^{(1)}_{max} + \left(\frac{\delta g_{bbh}}{g_{bbh}}\right)^{(2)}_{max}, \tag{38}$$

where the leading order term in M_{EW}/M_S is $\mathcal{O}(1)$,

$$\left(\frac{\delta g_{bbh}}{g_{bbh}}\right)^{(1)}_{max} = \frac{\alpha_s(\mu_R)}{3\pi}\frac{M_{\tilde{g}}(X_b - Y_b)}{M_S^2} f_1(R)\,, \tag{39}$$

with $Y_b \equiv A_b + \mu\cot\alpha$ and $R \equiv M_{\tilde{g}}/M_S$. Eq. 39 only decouples for large M_S if the additional limit $M_A \to \infty$ is also taken[23, 28]. In this limit,

$$X_b - Y_b \to \frac{2\mu M_Z^2}{M_A^2}\tan\beta\cos 2\beta + \mathcal{O}\left(\frac{M_{EW}^4}{M_A^4}\right). \tag{40}$$

The subleading terms of $\mathcal{O}(M_{EW}^2/M_S^2)$ are,[8]

$$\begin{aligned}\left(\frac{\delta g_{bbh}}{g_{bbh}}\right)^{(2)}_{max} \;=\; & \frac{\alpha_s(\mu_R)}{3\pi}\Bigg\{-\frac{M_{\tilde{g}}Y_b}{M_S^2}\left[\frac{M_h^2}{12M_S^2}f_3^{-1}(R) + \frac{X_b^2 m_b^2}{2(1+\Delta_b)^2 M_S^4}f_3(R)\right] \\ & -\frac{m_b^2 X_b Y_b}{2(1+\Delta_b)^2 M_S^4}f_3^{-1}(R) \\ & +\frac{M_Z^2}{3M_S^2}\frac{c_\beta s_{\alpha+\beta}}{s_\alpha}I_3^b\left[3f_1(R) + \left(\frac{2M_{\tilde{g}}X_b}{M_S^2} - 1\right)f_2(R)\right]\Bigg\}\end{aligned} \tag{41}$$

The functions $f_i(R)$ are defined in Appendix C.

The $\frac{s}{M_S^2}$, $\frac{u}{M_S^2}$ terms in Eq. 37 are not a rescaling of the lowest order vertex and cannot be obtained from the effective Lagrangian. We find,

$$\delta\kappa_{max} = \frac{1}{4}\left[f_3(R) + \frac{1}{9}f_3^{-1}(R)\right] - R\frac{Y_b}{2M_S}\left[f_2'(R) + \frac{1}{9}\hat{f}_2(R)\right]. \tag{42}$$

The $\delta\kappa_{max}$ term is $\mathcal{O}(1)$ in M_{EW}/M_S and has its largest values for small R and large ratios of Y_b/M_S, as can be seen in Fig. 2. Large effects can be obtained for $Y_b/M_S \sim 10$ and $M_{\tilde{g}} << M_S$. However, the parameters must be carefully tuned so that $A_b/M_S \lesssim 1$ in order not to break color[45].

The amplitude squared, summing over final state spins and colors and averaging over initial state spins and colors, including one-loop SQCD corrections is

$$\left|\overline{\mathcal{A}}\right|^2_{max} \;=\; -\frac{2\pi\alpha_s(\mu_R)}{3}g_{bbh}^2\left[\left(\frac{u^2+M_h^4}{st}\right)\left[1 + 2\left(\frac{\delta g_{bbh}}{g_{bbh}}\right)_{max}\right] + \frac{\alpha_s(\mu_R)}{2\pi}\frac{M_h^2}{M_S^2}\delta\kappa_{max}\right]. \tag{43}$$

[8] We use the shorthand, $c_\beta = \cos\beta$, $s_{\alpha+\beta} = \sin(\alpha+\beta)$, etc.

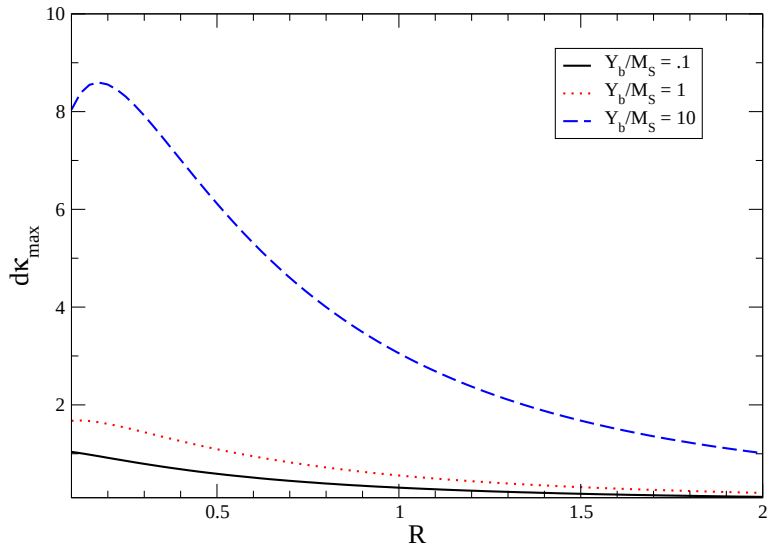


FIG. 2: Contribution of $\delta\kappa_{max}$ defined in Eq. 42 as a function of $R = M_{\tilde{g}}/M_S$.

Note that in the cross section, the $\delta\kappa_{max}$ term is not enhanced by a power of s and gives a contribution of $\mathcal{O}\left(\frac{M_{EW}^2}{M_S^2}\right)$.

Expanding Δ_b in the maximal mixing limit,

$$\Delta_b \to -\frac{\alpha_s(\mu_S)}{3\pi}\frac{M_{\tilde{g}}\mu}{M_S^2}\tan\beta f_1(R) + \mathcal{O}\left(\frac{M_{EW}^4}{M_S^4}\right). \tag{44}$$

By comparison with Eq. 14,

$$\begin{aligned}\left|\overline{\mathcal{A}}\right|^2_{max} &= -\frac{2\pi\alpha_s(\mu_R)}{3}(g_{bbh}^{\Delta_b})^2\left\{\left(\frac{u^2+M_h^4}{st}\right)\left[1+2\left(\frac{\delta g_{bbh}}{g_{bbh}}\right)^{(2)}_{max}\right]\right. \\ &\left. +\frac{\alpha_s(\mu_R)}{2\pi}\frac{M_h^2}{M_S^2}\delta\kappa_{max}\right\} + \mathcal{O}\left(\left[\frac{M_{EW}}{M_S}\right]^4, \alpha_s^3\right).\end{aligned} \tag{45}$$

Note that the mis-match in the arguments of α_s in Eqs. 44 and 45 is higher order in α_s than the terms considered here. The $(\delta g_{bbh}/g_{bbh})^{(2)}_{max}$ and $\delta\kappa_{max}$ terms both correspond to contributions which are not present in the effective Lagrangian approach. These terms are, however, suppressed by powers of M_{EW}^2/M_S^2 and the non-decoupling effects discussed in Refs. [28] and [27] are completely contained in the $g_{bbh}^{\Delta_b}$ term.

B. Minimal Mixing in the b Squark Sector

The minimal mixing scenario is characterized by a mass splitting between the b squarks which is of order the b squark mass, $\mid M^2_{\tilde{b}_1} - M^2_{\tilde{b}_2} \mid \sim M^2_S$. In this case,

$$\mid \tilde{m}^2_L - \tilde{m}^2_R \mid >> \frac{m_b \mid X_b \mid}{(1+\Delta_b)}\,, \tag{46}$$

and the mixing angle in the b squark sector is close to zero,

$$\cos 2\tilde{\theta}_b \sim 1 - \frac{2m_b^2 X_b^2}{(M^2_{\tilde{b}_1} - M^2_{\tilde{b}_2})^2}\left(\frac{1}{1+\Delta_b}\right)^2. \tag{47}$$

The non-zero subamplitudes are

$$\begin{aligned}
A_s &= -g_s T^A g_{bbh} M_s^\mu \left\{1 + \left(\frac{\delta g_{bbh}}{g_{bbh}}\right)_{min} + \frac{\alpha_s(\mu_R)}{4\pi}\frac{s}{\tilde{M}_g^2}\delta\kappa_{min}\right\} \\
A_t &= -g_s T^A g_{bbh} M_t^\mu \left\{1 + \left(\frac{\delta g_{bbh}}{g_{bbh}}\right)_{min}\right\} \\
A_1 &= -g_s T^A g_{bbh} M_1^\mu \left(-\frac{\alpha_s(\mu_R) u}{2\pi \tilde{M}_g^2}\right)\delta\kappa_{min}\,.
\end{aligned} \tag{48}$$

Expanding the exact one-loop results of Appendix B in the minimal mixing scenario,

$$\delta\kappa_{min} = \frac{1}{8}\Sigma_{i=1}^2\left(R_i^2\left[\frac{1}{9}f_3^{-1}(R_i) + f_3(R_i)\right]\right) + \frac{Y_b}{M_{\tilde{g}}}\frac{R_1^2 R_2^2}{R_2^2 - R_1^2}\left(3h_1(R_1,R_2,1) + \frac{8}{3}h_1(R_1,R_2,2)\right), \tag{49}$$

where $R_i = M_{\tilde{g}}/M_{\tilde{b}_i}$ and the functions $f_i(R_i)$ and $h_i(R_1,R_2,n)$ are defined in Appendix C. The $\delta\kappa_{min}$ function is shown in Fig. 3. For large values of $Y_b/M_{\tilde{g}}$ it can be significantly larger than 1.

As in the previous section, the spin and color averaged amplitude-squared is,

$$\mid \overline{A} \mid^2_{min} = -\frac{2\alpha_s(\mu_R)\pi}{3}(g^2_{bbh})\left\{\frac{(M_h^4 + u^2)}{st}\left[1 + 2\left(\frac{\delta g_{bbh}}{g_{bbh}}\right)_{min}\right] + \frac{\alpha_s(\mu_R)}{2\pi}\delta\kappa_{min}\frac{M_h^2}{M_{\tilde{g}}^2}\right\}, \tag{50}$$

with,

$$\left(\frac{\delta g_{bbh}}{g_{bbh}}\right)_{min} = \left(\frac{\delta g_{bbh}}{g_{bbh}}\right)^{(1)}_{min} + \left(\frac{\delta g_{bbh}}{g_{bbh}}\right)^{(2)}_{min}. \tag{51}$$

The leading order term in M_{EW}/M_S is $\mathcal{O}(1)$,

$$\left(\frac{\delta g_{bbh}}{g_{bbh}}\right)^{(1)}_{min} = \frac{2\alpha_s(\mu_R)}{3\pi}\frac{(X_b - Y_b)}{M_{\tilde{g}}}\frac{R_1^2 R_2^2}{R_1^2 - R_2^2}h_1(R_1,R_2,0)\,. \tag{52}$$

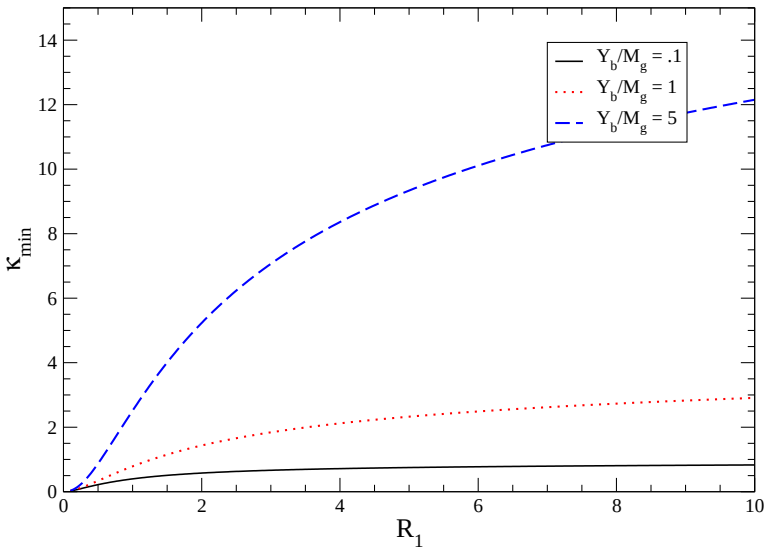


FIG. 3: Contribution of $\delta\kappa_{min}$ defined in Eq. 49 as a function of $R_i = M_{\tilde{g}}/M_{\tilde{b}_i}$.

The subleading terms are $\mathcal{O}\left(\frac{M_{EW}^2}{M_S^2}\right)$,

$$\begin{aligned}
\left(\frac{\delta g_{bbh}}{g_{bbh}}\right)^{(2)}_{min} &= \frac{\alpha_s}{4\pi}\Bigg\{-\frac{8M_{\tilde{g}}Y_b}{3\Delta M^2_{\tilde{b}_{12}}}\Bigg[\frac{h_2\left(R_1,R_2\right)M_h^2}{\Delta M^2_{\tilde{b}_{12}}} \\
&+\frac{m_b^2X_b^2}{\left(\Delta M^2_{\tilde{b}_{12}}\right)^2(1+\Delta_b)^2}\left\{2\mathcal{S}\left(\frac{f_1\left(R\right)}{M^2_{\tilde{b}}}\right)+\frac{h_1\left(R_1,R_2,0\right)}{\Delta M^2_{\tilde{b}_{12}}}\right\}\Bigg] \\
&+\frac{4}{3}\frac{c_\beta s_{\alpha+\beta}}{s_\alpha}I_3^bM_Z^2\left[\mathcal{S}\left(\frac{3f_1\left(R\right)-f_2\left(R\right)}{3M^2_{\tilde{b}}}\right)-\frac{2M_{\tilde{g}}X_b}{\Delta M^2_{\tilde{b}_{12}}}\mathcal{A}\left(\frac{f_1\left(R\right)}{M^2_{\tilde{b}}}\right)\right] \\
&+\frac{4}{3}\frac{c_\beta s_{\alpha+\beta}}{s_\alpha}\left(I_3^b-2Q^bs_W^2\right)M_Z^2\Bigg[\mathcal{A}\left(\frac{3f_1\left(R\right)-f_2\left(R\right)}{3M^2_{\tilde{b}}}\right) \\
&-\frac{2M_{\tilde{g}}X_b}{\Delta M^2_{\tilde{b}_{12}}}\left\{\mathcal{S}\left(\frac{f_1\left(R\right)}{M^2_{\tilde{b}}}\right)+\frac{h_1\left(R_1,R_2,0\right)}{\Delta M^2_{\tilde{b}_{12}}}\right\}\Bigg] \\
&+\frac{8}{3}\frac{m_b^2X_bY_b}{\Delta M^2_{\tilde{b}_{12}}(1+\Delta_b)^2}\mathcal{A}\left(\frac{3f_1\left(R\right)-f_2\left(R\right)}{3M^2_{\tilde{b}}}\right)\Bigg\}. \qquad (53)
\end{aligned}$$

The symmetric and anti-symmetric functions are defined,

$$\begin{aligned}
\mathcal{S}(f(R,M_{\tilde{b}}) &\equiv \frac{1}{2}\Big[f(R_1,M_{\tilde{b}_1})+f(R_2,M_{\tilde{b}_2})\Big] \\
\mathcal{A}(f(R,M_{\tilde{b}}) &\equiv \frac{1}{2}\Big[f(R_1,M_{\tilde{b}_1})-f(R_2,M_{\tilde{b}_2})\Big] \qquad (54)
\end{aligned}$$

and $\Delta M^2_{\tilde{b}_{12}} \equiv M^2_{\tilde{b}_1} - M^2_{\tilde{b}_2}$. The remaining functions are defined in Appendix C.

By expanding Δ_b in the minimal mixing limit, we find the analogous result to that of the maximal mixing case,

$$\begin{aligned} \mid \overline{A} \mid^2_{min} \;=\; & -\frac{2\alpha_s\pi}{3}(g^{\Delta_b}_{bbh})^2\Bigg\{\frac{(M_h^4+u^2)}{st}\Bigg[1+2\left(\frac{\delta g_{bbh}}{g_{bbh}}\right)^{(2)}_{min}\Bigg] \\ & +\frac{\alpha_s}{2\pi}\delta\kappa_{min}\frac{M_h^2}{M_{\tilde{g}}^2}\Bigg\} + \mathcal{O}\left(\left[\frac{M_{EW}}{M_S}\right]^4, \alpha_s^3\right). \end{aligned} \tag{55}$$

The contributions which are not contained in σ_{IBA} are again found to be suppressed by $\mathcal{O}\left(\left[\frac{M_{EW}}{M_S}\right]^2\right)$.

IV. NUMERICAL RESULTS

We present results for $pp \to b(\overline{b})h$ at $\sqrt{s} = 7\ TeV$ with $p_{Tb} > 20\ GeV$ and $\mid \eta_b \mid < 2.0$. We use FeynHiggs to generate M_h and $\sin\alpha_{eff}$ and then iteratively solve for the b squark masses and Δ_b from Eqs. 12 and 19. We evaluate the 2-loop $\overline{MS}$ b mass at $\mu_R = M_h/2$, which we also take to be the renormalization and factorization scales[9]. Finally, Figs 4, 5, 6, and 7 use the CTEQ6m NLO parton distribution functions[46]. Figs. 4, 5 and 6 show the percentage deviation of the complete one-loop SQCD calculation from the Improved Born Approximation of Eq. 16 for $\tan\beta = 40$ and $\tan\beta = 20$ and representative values of the MSSM parameters[10]. In both extremes of b squark mixing, the Improved Born Approximation approximation is within a few percent of the complete one-loop SQCD calculation and so is a reliable prediction for the rate. This is true for both large and small M_A. In addition, the large M_S expansion accurately reproduces the full SQCD one-loop result to within a few percent. These results are expected from the expansions of Eqs. 45 and 55, since the terms which differ between the Improved Born Approximation and the one-loop calculation are suppressed in the large M_S limit.

Fig. 7 compares the total SQCD rate for maximal and minimal mixing, which bracket the allowed mixing possibilities. For large M_S, the effect of the mixing is quite small, while for $M_S \sim 800\ GeV$, the mixing effects are at most a few fb. The accuracy of the Improved Born Approximation as a function of m_R is shown in Fig. 8 for fixed M_A, μ, and m_L. As

[9] Δ_b is evaluated using $\alpha_s(M_S)$.
[10] Figs. 4, 5 and 6 do not include the pure QCD NLO corrections[17].

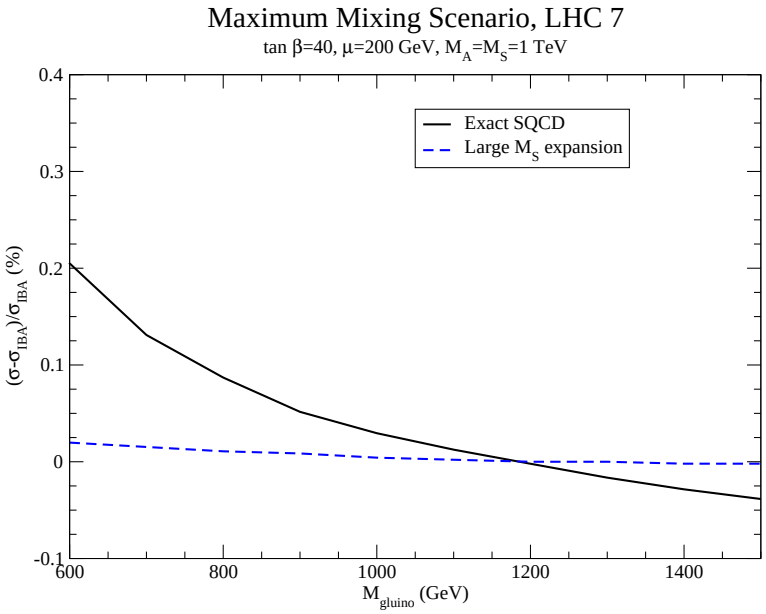


FIG. 4: Percentage difference between the Improved Born Approximation and the exact one-loop SQCD calculation of $pp \to bh$ for maximal mixing in the b-squark sector at $\sqrt{s} = 7\,TeV$, $\tan\beta = 40$, and $M_A = 1\ TeV$.

m_R is increased, the effects become very tiny. Even for light gluino masses, the Improved Born Approximation reproduces the exact SQCD result to within a few percent.

In Fig. 9, we show the scale dependence for the total rate, including NLO QCD and SQCD corrections (dotted lines) for a representative set of MSSM parameters at $\sqrt{s} = 7\ TeV$. The NLO scale dependence is quite small when $\mu_R = \mu_F \sim M_h$. However, there is a roughly $\sim 5\%$ difference between the predictions found using the CTEQ6m PDFs and the MSTW2008 NLO PDFs[47]. In Fig. 10, we show the scale dependence for small μ_F (as preferred by [16]), and see that it is significantly larger than in Fig. 9. This is consistent with the results of [19, 29].

V. CONCLUSION

Our major results are the analytic expressions for the SQCD corrections to b Higgs associated production in the minimal (Eqs. 41, 42 and 45) and maximal (Eqs. 49, 53 and 55) b squark mixing scenarios for large $\tan\beta$ and squark masses,M_S. These results

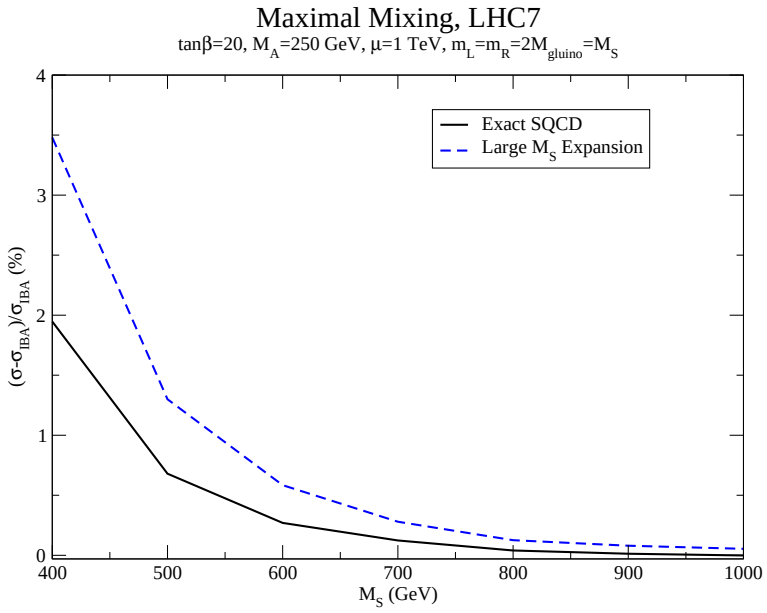


FIG. 5: Percentage difference between the Improved Born Approximation and the exact one-loop SQCD calculation of $pp \to bh$ for maximal mixing in the b-squark sector at $\sqrt{s} = 7\ TeV$, $\tan\beta = 20$, and $M_A = 250\ GeV$.

clearly demonstrate that deviations from the Δ_b approximation are suppressed by powers of (M_{EW}/M_S) in the large $\tan\beta$ region. The Δ_b approximation hence yields an accurate prediction in the 5 flavor number scheme for the cross section for squark and gluino masses at the TeV scale. As a by-product of our calculation, we update the predictions for b Higgs production at $\sqrt{s} = 7\ TeV$.

Acknowledgements

S. Dawson and P.Jaiswal are supported by the United States Department of Energy under Grant DE-AC02-98CH10886.

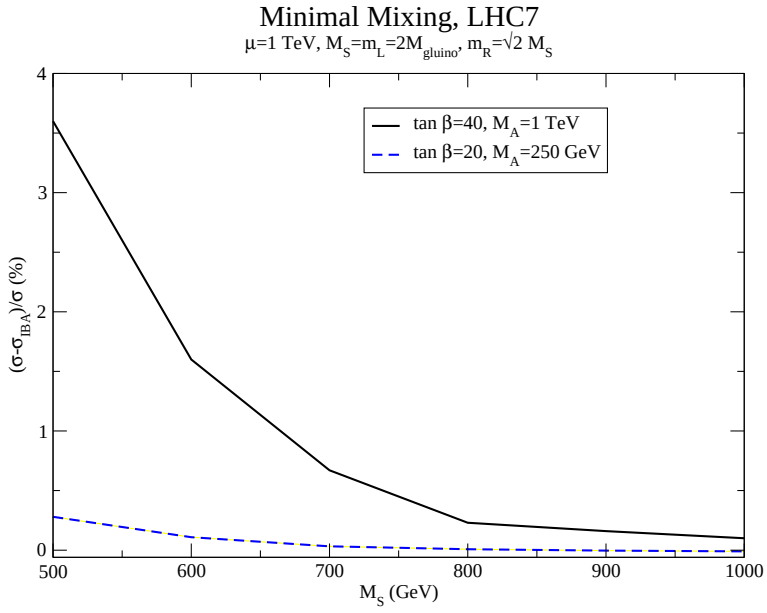


FIG. 6: Percentage difference between the Improved Born Approximation and the exact one-loop SQCD calculation for $pp \to bh$ for minimal mixing in the b squark sector at $\sqrt{s} = 7\ TeV$.

Appendix A: Passarino-Veltman Functions

The scalar integrals are defined as:

$$\begin{aligned}
\frac{i}{16\pi^2} A_0(M_0^2) &= \int \frac{d^n k}{(2\pi)^n} \frac{1}{N_0}\,, \\
\frac{i}{16\pi^2} B_0(p_1^2; M_0^2, M_1^2) &= \int \frac{d^n k}{(2\pi)^n} \frac{1}{N_0 N_1}\,, \\
\frac{i}{16\pi^2} C_0(p_1^2, p_2^2, (p_1+p_2)^2; M_0^2, M_1^2, M_2^2) &= \int \frac{d^n k}{(2\pi)^n} \frac{1}{N_0 N_1 N_2}\,, \\
\frac{i}{16\pi^2} D_0(p_1^2, p_2^2, p_3^2, p_4^2, (p_1+p_2)^2, (p_2+p_3)^2; M_0^2, M_1^2, M_2^2, M_3^2) & \\
= \int \frac{d^n k}{(2\pi)^n} \frac{1}{N_0 N_1 N_2 N_3}\,, & \qquad (56)
\end{aligned}$$

where,

$$\begin{aligned}
N_0 &= k^2 - M_0^2 \\
N_1 &= (k+p_1)^2 - M_1^2 \\
N_2 &= (k+p_1+p_2)^2 - M_2^2 \\
N_3 &= (k+p_1+p_2+p_3)^2 - M_3^2\,. \qquad (57)
\end{aligned}$$

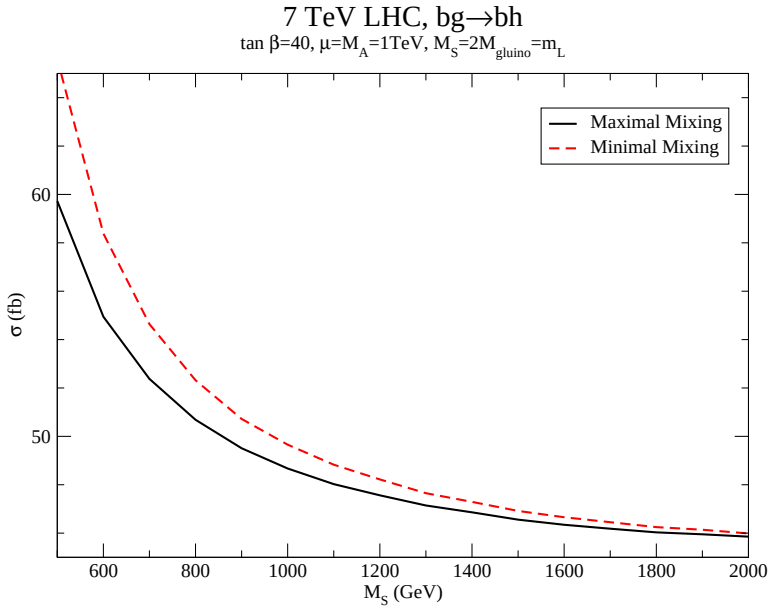


FIG. 7: Comparison between the exact one-loop SQCD calculation for $pp \to bh$ for minimal and maximal mixing in the b squark sector at $\sqrt{s} = 7\ TeV$ and $\tan\beta = 40$. The minimal mixing curve has $m_R = \sqrt{2}M_S$ and $\tilde{\theta}_b \sim 0$, while the maximal mixing curve has $m_R = M_S$ and $\tilde{\theta}_b \sim \frac{\pi}{4}$.

The tensor integrals encountered are expanded in terms of the external momenta p_i and the metric tensor $g^{\mu\nu}$. For the two-point function we write:

$$\begin{aligned} \frac{i}{16\pi^2} B^\mu(p_1^2; M_0^2, M_1^2) &= \int \frac{d^n k}{(2\pi)^n} \frac{k^\mu}{N_0 N_1} \\ &\equiv \frac{i}{16\pi^2} p_1^\mu B_1(p_1^2, M_0^2, M_1^2)\,, \end{aligned} \tag{58}$$

while for the three-point functions we have both rank-one and rank-two tensor integrals which we expand as:

$$\begin{aligned} C^\mu(p_1^2, p_2^2, (p_1+p_2)^2; M_0^2, M_1^2, M_2^2) &= p_1^\mu C_{11} + p_2^\mu C_{12}\,, \\ C^{\mu\nu}(p_1^2, p_2^2, (p_1+p_2)^2; M_0^2, M_1^2, M_2^2) &= p_1^\mu p_1^\nu C_{21} + p_2^\mu p_2^\nu C_{22} \\ &+ (p_1^\mu p_2^\nu + p_1^\nu p_2^\mu) C_{23} + g^{\mu\nu} C_{24}\,, \end{aligned} \tag{59}$$

where:

$$\frac{i}{16\pi^2} C^\mu(C^{\mu\nu})(p_1^2, p_2^2, (p_1+p_2)^2; M_0^2, M_1^2, M_2^2) \equiv \int \frac{d^n k}{(2\pi)^n} \frac{k^\mu (k^\mu k^\nu)}{N_0 N_1 N_2} \tag{60}$$

Finally, for the box diagrams, we encounter rank-one and rank-two tensor integrals which

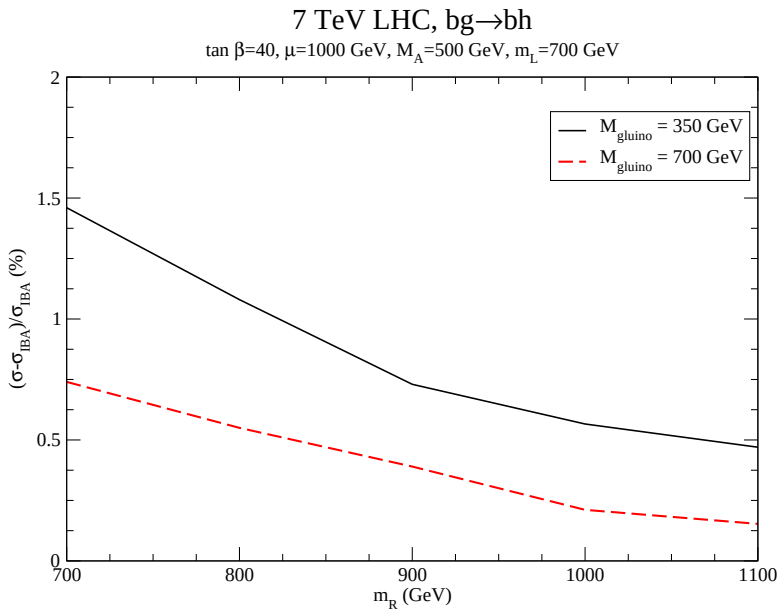


FIG. 8: Percentage difference between the Improved Born Approximation and the exact one-loop SQCD calculation for $pp \to bh$ as a function of m_R at $\sqrt{s} = 7\ TeV$ and $\tan\beta = 40$.

are written in terms of the Passarino-Veltmann coefficients as:

$$\frac{i}{16\pi^2} D^{\mu}(p_1^2, p_2^2, p_3^2, p_4^2, (p_1+p_2)^2, (p_2+p3)^2; M_0^2, M_1^2, M_2^2) \equiv \int \frac{d^n k}{(2\pi)^n} \frac{k^{\mu}}{N_0 N_1 N_2 N_3}$$
$$= \frac{i}{16\pi^2} \left\{ p_1^{\mu} D_{11} + p_2^{\mu} D_{12} + p_3^{\mu} D_{13} \right\}. \tag{61}$$

$$\frac{i}{16\pi^2} D^{\mu\nu}(p_1^2, p_2^2, p_3^2, p_4^2, (p_1+p_2)^2, (p_2+p_3)^2; M_0^2, M_1^2, M_2^2) \equiv \int \frac{d^n k}{(2\pi)^n} \frac{k^{\mu} k^{\nu}}{N_0 N_1 N_2 N_3}$$
$$= \frac{i}{16\pi^2} \left\{ g^{\mu\nu} D_{00} + \text{tensor structures not needed here} \right\}. \tag{62}$$

Appendix B: One-Loop Results

In this appendix we give the non-zero contributions of the individual diagrams in terms of the basis functions of Eq. 20 and the decompositions of Eq. 22. The contributions proportional to $m_b \tan\beta$ are new and were not included in the results of Ref.[23]. Although we specialize to the case of the lightest Higgs boson, h, our results are easily generalized to the heavier neutral Higgs boson, H, and so the Feynman diagrams in this appendix are shown for $\phi_i = h, H$.

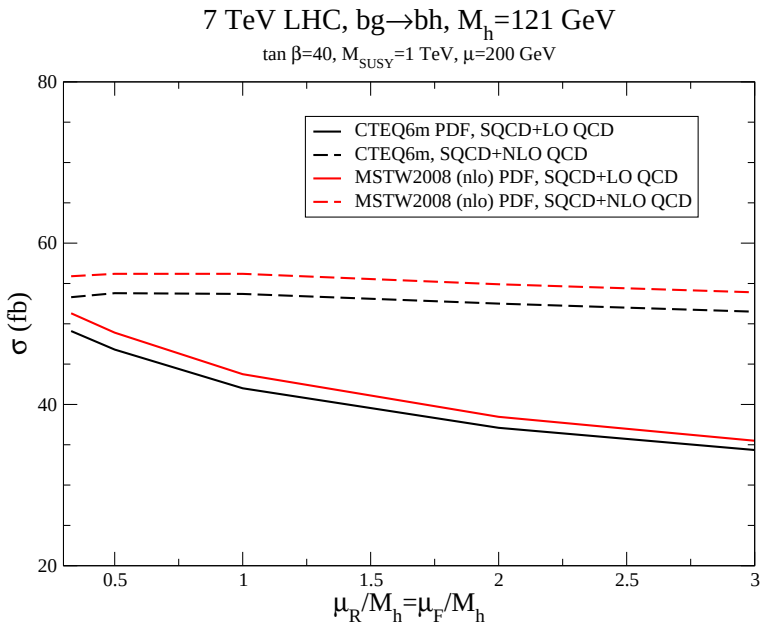


FIG. 9: Total cross section for $pp \to b(\bar{b})h$ production including NLO QCD and SQCD corrections (dotted lines) as a function of renormalization/factorization scale using CTEQ6m (black) and MSTW2008 NLO (red) PDFs. We take $M_{\tilde{g}} = 1\ TeV$ and the remaining MSSM parameters as in Fig. 4.

The self-energy diagrams of Fig. 11:

$$\begin{aligned} X_{S_1}^{(t)} &= \frac{4}{3}\sum_{i=1}^{2}\left\{B_1 - (-1)^i \frac{2m_b M_{\tilde{g}} s_{2\tilde{b}}}{t} B_0\right\}\left(M_{\tilde{b}_i}^2\right) \\ X_{S_1}^{(2)} &= -\frac{4}{3}\sum_{i=1}^{2}(-1)^i \frac{m_b M_{\tilde{g}} s_{2\tilde{b}}}{t} B_0\left(M_{\tilde{b}_i}^2\right) \end{aligned} \tag{63}$$

where we have have used the shorthand notation for the arguments of Passarino-Veltman functions, $B_{0,1}\left(M_{\tilde{b}_i}^2\right) \equiv B_{0,1}\left(t; M_{\tilde{g}}^2, M_{\tilde{b}_i}^2\right)$.

$$\begin{aligned} X_{S_2}^{(s)} &= \frac{4}{3}\sum_{i=1}^{2}\left\{B_1 - (-1)^i \frac{2m_b M_{\tilde{g}} s_{2\tilde{b}}}{s} B_0\right\}\left(M_{\tilde{b}_i}^2\right) \\ X_{S_2}^{(2)} &= -\frac{4}{3}\sum_{i=1}^{2}(-1)^i \frac{m_b M_{\tilde{g}} s_{2\tilde{b}}}{s} B_0\left(M_{\tilde{b}_i}^2\right) \end{aligned} \tag{64}$$

and $B_{0,1}\left(M_{\tilde{b}_i}^2\right) \equiv B_{0,1}\left(s; M_{\tilde{g}}^2, M_{\tilde{b}_i}^2\right)$

The vertex functions of Fig. 12:

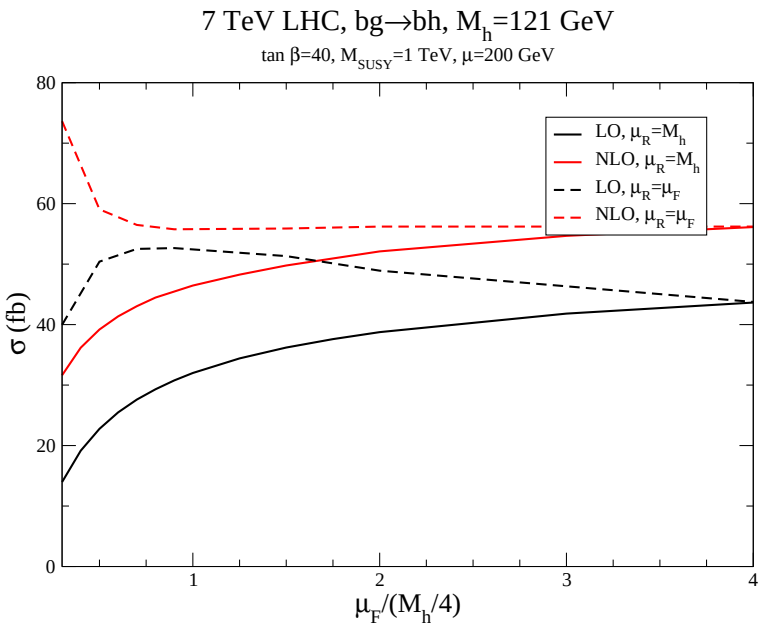


FIG. 10: Total cross section for $pp \to b(\bar{b})h$ production including NLO QCD and SQCD corrections as a function of the factorization scale using MSTW2008 NLO PDFs. We take $M_{\tilde{g}} = 1\ TeV$ and the remaining MSSM parameters as in Fig. 4.

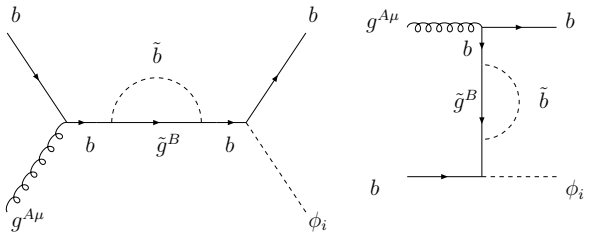


FIG. 11: Self-energy diagrams, S_1 and S_2.

Diagram V_1:

$$
\begin{aligned}
X_{V_1}^{(s)} &= \frac{s}{6}\sum_{i=1}^{2}\left\{C_{12}+C_{23}-(-1)^i\,\frac{2m_b M_{\tilde{g}} s_{2\tilde{b}}}{t}\,(C_0+C_{11})\right\}\left(M_{\tilde{b}_i}^2\right)\\
X_{V_1}^{(t)} &= -\frac{1}{6}\sum_{i=1}^{2}\left\{t\,(C_{12}+C_{23})+2C_{24}-(-1)^i\,2m_b M_{\tilde{g}} s_{2\tilde{b}}\,(C_0+C_{11})\right\}\left(M_{\tilde{b}_i}^2\right)\\
X_{V_1}^{(1)} &= -\frac{u}{3}\sum_{i=1}^{2}\left\{C_{12}+C_{23}-(-1)^i\,\frac{2m_b M_{\tilde{g}} s_{2\tilde{b}}}{t}\,(C_0+C_{11})\right\}\left(M_{\tilde{b}_i}^2\right)\\
X_{V_1}^{(3)} &= -\frac{1}{3}\sum_{i}(-1)^i\,m_b M_{\tilde{g}} s_{2\tilde{b}}\,(C_0+C_{11})\left(M_{\tilde{b}_i}^2\right)
\end{aligned}
\tag{65}
$$

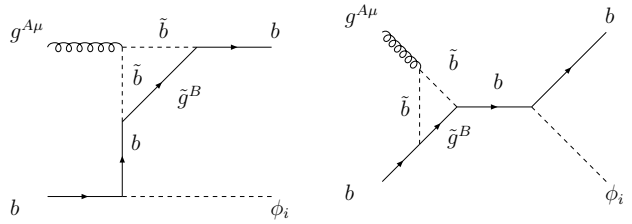


FIG. 12: Virtual diagrams, V_1 and V_2.

where $C_{0,11,12,23,24}\left(M^2_{\tilde{b}_i}\right) \equiv C_{0,11,12,23,24}\left(0,0,t;M^2_{\tilde{g}},M^2_{\tilde{b}_i},M^2_{\tilde{b}_i}\right)$.

Diagram V_2:

$$\begin{aligned}
X^{(s)}_{V_2} &= -\frac{1}{3}\sum_{i=1}^{2} C_{24}\left(M^2_{\tilde{b}_i}\right) \\
X^{(1)}_{V_2} &= -\frac{u}{3}\sum_{i=1}^{2}\left\{C_{12}+C_{23}-(-1)^i\,\frac{2m_b M_{\tilde{g}} s_{2\tilde{b}}}{s}\left(C_0+C_{11}\right)\right\}\left(M^2_{\tilde{b}_i}\right) \\
X^{(4)}_{V_2} &= \frac{1}{3}\sum_{i}(-1)^i\, m_b M_{\tilde{g}} s_{2\tilde{b}}\left(C_0+C_{11}\right)\left(M^2_{\tilde{b}_i}\right)
\end{aligned} \tag{66}$$

where $C_{0,11,12,23,24}\left(M^2_{\tilde{b}_i}\right) \equiv C_{0,11,12,23,24}\left(0,0,s;M^2_{\tilde{g}},M^2_{\tilde{b}_i},M^2_{\tilde{b}_i}\right)$.

The vertex functions of Fig. 13:

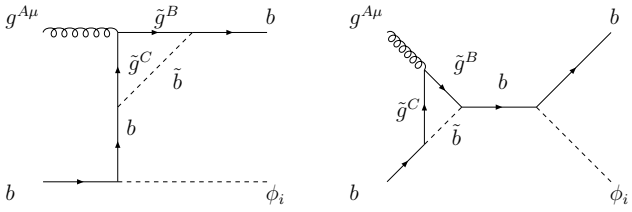


FIG. 13: Virtual diagrams, V_3 and V_4.

Diagram V_3:

$$
\begin{aligned}
X_{V_3}^{(s)} &= \frac{3s}{2}\sum_{i=1}^{2}\left\{C_{12}+C_{23}-(-1)^i\,\frac{2m_bM_{\tilde{g}}s_{2\tilde{b}}}{t}\left(C_0+C_{12}\right)\right\}\left(M_{\tilde{b}_i}^2\right)\\
X_{V_3}^{(t)} &= -\frac{3}{2}\sum_{i=1}^{2}\left\{M_{\tilde{g}}^2C_0-2\left(1-\epsilon\right)C_{24}-(-1)^i\,2m_bM_{\tilde{g}}s_{2\tilde{b}}C_{12}\right\}\left(M_{\tilde{b}_i}^2\right)\\
X_{V_3}^{(1)} &= -3u\sum_{i=1}^{2}\left\{C_{12}+C_{23}-(-1)^i\,\frac{2m_bM_{\tilde{g}}s_{2\tilde{b}}}{t}\left(C_0+C_{12}\right)\right\}\left(M_{\tilde{b}_i}^2\right)\\
X_{V_3}^{(2)} &= -\frac{3}{2}\sum_{i=1}^{2}(-1)^i\,m_bM_{\tilde{g}}s_{2\tilde{b}}C_0\left(M_{\tilde{b}_i}^2\right)\\
X_{V_3}^{(3)} &= -3\sum_{i=1}^{2}(-1)^i\,m_bM_{\tilde{g}}s_{2\tilde{b}}\left\{C_0+C_{12}\right\}\left(M_{\tilde{b}_i}^2\right)
\end{aligned}
\tag{67}
$$

where $C_{0,11,12,23,24}\left(M_{\tilde{b}_i}^2\right)\equiv C_{0,11,12,23,24}\left(0,0,t;M_{\tilde{g}}^2,M_{\tilde{g}}^2,M_{\tilde{b}_i}^2\right)$.

Diagram V_4:

$$
\begin{aligned}
X_{V_4}^{(s)} &= -\frac{3}{2}\sum_{i=1}^{2}\left\{M_{\tilde{g}}^2C_0-2\left(1-\epsilon\right)C_{24}-s\left(C_{12}+C_{23}\right)+(-1)^i\,2m_bM_{\tilde{g}}s_{2\tilde{b}}C_0\right\}\left(M_{\tilde{b}_i}^2\right)\\
X_{V_4}^{(1)} &= -3u\sum_{i=1}^{2}\left\{C_{12}+C_{23}-(-1)^i\,\frac{2m_bM_{\tilde{g}}s_{2\tilde{b}}}{s}\left(C_0+C_{12}\right)\right\}\left(M_{\tilde{b}_i}^2\right)\\
X_{V_4}^{(2)} &= -\frac{3}{2}\sum_{i=1}^{2}(-1)^i\,m_bM_{\tilde{g}}s_{2\tilde{b}}C_0\left(M_{\tilde{b}_i}^2\right)\\
X_{V_4}^{(4)} &= 3\sum_{i=1}^{2}(-1)^i\,m_bM_{\tilde{g}}s_{2\tilde{b}}\left\{C_0+C_{12}\right\}\left(M_{\tilde{b}_i}^2\right)
\end{aligned}
\tag{68}
$$

where $C_{0,11,12,23,24}\left(M_{\tilde{b}_i}^2\right)\equiv C_{0,11,12,23,24}\left(0,0,s;M_{\tilde{g}}^2,M_{\tilde{g}}^2,M_{\tilde{b}_i}^2\right)$.

The vertex functions of Fig. 14:

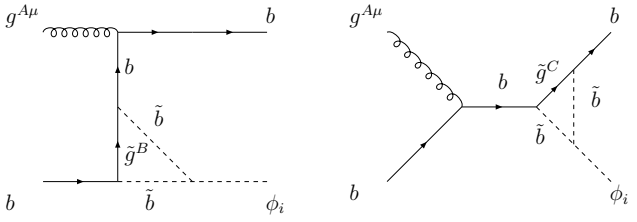


FIG. 14: Virtual diagrams, V_5 and V_6.

Diagram V_5:

$$X_{V_5}^{(t)} = \frac{4}{3}\sum_{i,j=1}^{2} C_{h,ij}\left\{\delta_{ij} m_b C_{11} + a_{ij} M_{\tilde{g}} C_0\right\}\left(M_{\tilde{b}_i}^2, M_{\tilde{b}_j}^2\right)$$
$$X_{V_5}^{(2)} = \frac{4}{3} m_b \sum_{i,j=1,2} C_{h,ij}\delta_{ij} C_{12}\left(M_{\tilde{b}_i}^2, M_{\tilde{b}_j}^2\right) \tag{69}$$

where $C_{0,11,12,23,24}\left(M_{\tilde{b}_i}^2, M_{\tilde{b}_j}^2\right) \equiv C_{0,11,12,23,24}\left(0, M_h^2, t; M_{\tilde{g}}^2, M_{\tilde{b}_i}^2, M_{\tilde{b}_j}^2\right)$, the squark mixing matrix is defined,

$$\begin{pmatrix} a_{11} & a_{12} \\ a_{21} & a_{22} \end{pmatrix} = \begin{pmatrix} s_{2\tilde{b}} & c_{2\tilde{b}} \\ c_{2\tilde{b}} & -s_{2\tilde{b}} \end{pmatrix} \tag{70}$$

and the light Higgs-squark-squark couplings $C_{h,ij}$, are normalized with respect to the Higgs-quark-quark coupling[2],

$$C_{h,11} + C_{h,22} = 4m_b + \frac{2M_Z^2}{m_b} I_3^b \frac{s_{\alpha+\beta} c_\beta}{s_\alpha} \tag{71}$$
$$C_{h,11} - C_{h,22} = 2Y_b s_{2\tilde{b}} + \frac{2M_Z^2}{m_b} c_{2\tilde{b}}\left(I_3^b - 2Q_b s_W^2\right)\frac{s_{\alpha+\beta} c_\beta}{s_\alpha} \tag{72}$$
$$C_{h,12} = C_{h,21} = Y_b c_{2\tilde{b}} - \frac{M_Z^2}{m_b} s_{2\tilde{b}}\left(I_3^b - 2Q^b s_W^2\right)\frac{s_{\alpha+\beta} c_\beta}{s_\alpha}, \tag{73}$$

$s_W^2 = \sin\theta_W^2 = 1 - M_W^2/M_Z^2$ and Y_b is defined below Eq. 41.

Diagram V_6:

$$X_{V_6}^{(s)} = \frac{4}{3}\sum_{i,j=1,2} C_{h,ij}\left\{\delta_{ij} m_b C_{11} + a_{ij} M_{\tilde{g}} C_0\right\}\left(M_{\tilde{b}_i}^2, M_{\tilde{b}_j}^2\right)$$
$$X_{V_6}^{(2)} = \frac{4}{3} m_b \sum_{i,j=1,2} C_{h,ij}\delta_{ij} C_{12}\left(M_{\tilde{b}_i}^2, M_{\tilde{b}_j}^2\right)$$
$$X_{V_6}^{(t)} = X_{V_6}^{(3)} = X_{V_6}^{(4)} = 0 \tag{74}$$

where $C_{0,11,12,23,24}\left(M_{\tilde{b}_i}^2, M_{\tilde{b}_j}^2\right) \equiv C_{0,11,12,23,24}\left(0, M_h^2, s; M_{\tilde{g}}^2, M_{\tilde{b}_i}^2, M_{\tilde{b}_j}^2\right)$.

The box diagram of Fig. 15:

$$X_{B_1}^{(s)} = \frac{3M_{\tilde{g}} s}{2}\sum_{i,j=1,2} a_{ij} C_{h,ij}\left\{D_0 + D_{13}\right\}\left(M_{\tilde{b}_i}^2, M_{\tilde{b}_j}^2\right)$$
$$X_{B_1}^{(t)} = -\frac{3M_{\tilde{g}} t}{2}\sum_{i,j=1,2} a_{ij} C_{h,ij} D_{13}\left(M_{\tilde{b}_i}^2, M_{\tilde{b}_j}^2\right)$$
$$X_{B_1}^{(1)} = 3M_{\tilde{g}} u \sum_{i,j=1,2} a_{ij} C_{h,ij}\left\{D_{11} - D_{13}\right\}\left(M_{\tilde{b}_i}^2, M_{\tilde{b}_j}^2\right)$$
$$X_{B_1}^{(2)} = -\frac{3m_b}{2}\sum_{i,j=1,2}\delta_{ij} C_{h,ij}\left\{M_{\tilde{g}}^2 D_0 - 2D_{00}\right\}\left(M_{\tilde{b}_i}^2, M_{\tilde{b}_j}^2\right) \tag{75}$$

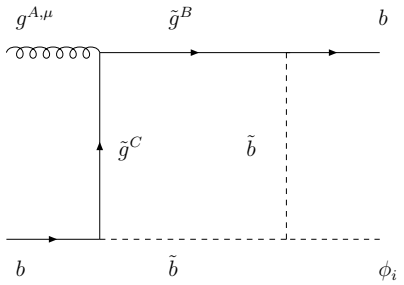


FIG. 15: Box diagram, B_1.

where, $D_0\left(M^2_{\tilde{b}_i}, M^2_{\tilde{b}_j}\right) \equiv D_0\left(0,0,0,M^2_h,s,t;M^2_{\tilde{b}_i},M^2_{\tilde{g}},M^2_{\tilde{g}},M^2_{\tilde{b}_j}\right)$.

The box diagram of Fig. 16:

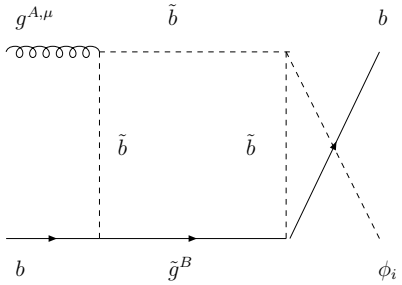


FIG. 16: Box diagram, B_2.

Diagram B_2:

$$
\begin{aligned}
X^{(s)}_{B_2} &= -\frac{M_{\tilde{g}}s}{6}\sum_{i,j=1,2} a_{ij}C_{h,ij}\left\{D_0+D_{11}\right\}\left(M^2_{\tilde{b}_i},M^2_{\tilde{b}_j}\right)\\
X^{(t)}_{B_2} &= \frac{M_{\tilde{g}}t}{6}\sum_{i,j=1,2} a_{ij}C_{h,ij}\left\{D_0+D_{11}\right\}\left(M^2_{\tilde{b}_i},M^2_{\tilde{b}_j}\right)\\
X^{(1)}_{B_2} &= \frac{M_{\tilde{g}}u}{3}\sum_{i,j=1,2} a_{ij}C_{h,ij}\left\{D_{11}-D_{12}\right\}\left(M^2_{\tilde{b}_i},M^2_{\tilde{b}_j}\right)\\
X^{(2)}_{B_2} &= -\frac{m_b}{3}\sum_{i,j=1,2} \delta_{ij}C_{h,ij}D_{00}\left(M^2_{\tilde{b}_i},M^2_{\tilde{b}_j}\right)
\end{aligned}
\tag{76}
$$

where $D_0\left(M^2_{\tilde{b}_i}, M^2_{\tilde{b}_j}\right) \equiv D_0\left(0,0,0,M^2_h,u,s;M^2_{\tilde{b}_i},M^2_{\tilde{g}},M^2_{\tilde{b}_j},M^2_{\tilde{b}_j}\right)$.

The box diagram of Fig. 17:

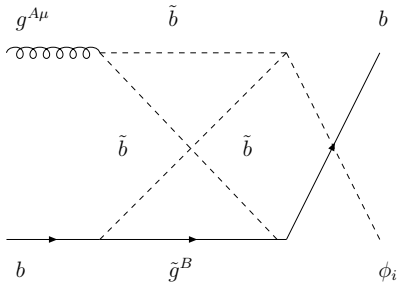


FIG. 17: Box diagram, B_3.

Diagram B_3:

$$\begin{aligned}
X_{B_3}^{(s)} &= \frac{M_{\tilde{g}} s}{6} \sum_{i,j=1,2} a_{ij} C_{h,ij} \left\{ D_0 + D_{12} \right\} \left(M_{\tilde{b}_i}^2, M_{\tilde{b}_j}^2 \right) \\
X_{B_3}^{(t)} &= -\frac{M_{\tilde{g}} t}{6} \sum_{i,j=1,2} a_{ij} C_{h,ij} \left\{ D_0 + D_{12} \right\} \left(M_{\tilde{b}_i}^2, M_{\tilde{b}_j}^2 \right) \\
X_{B_3}^{(1)} &= \frac{M_{\tilde{g}} u}{3} \sum_{i,j=1,2} a_{ij} C_{h,ij} \left\{ D_{11} - D_{12} \right\} \left(M_{\tilde{b}_i}^2, M_{\tilde{b}_j}^2 \right) \\
X_{B_3}^{(2)} &= -\frac{m_b}{3} \sum_{i,j=1,2} \delta_{ij} C_{h,ij} D_{00} \left(M_{\tilde{b}_i}^2, M_{\tilde{b}_j}^2 \right)
\end{aligned} \tag{77}$$

where $D_0 \left(M_{\tilde{b}_i}^2, M_{\tilde{b}_j}^2 \right) \equiv D_0 \left(0, 0, 0, M_h^2, u, t; M_{\tilde{b}_i}^2, M_{\tilde{g}}^2, M_{\tilde{b}_j}^2, M_{\tilde{b}_j}^2 \right)$.

The vertex and external wavefunction counter terms, Eq. 29, along with the subtraction of Eq. 32, give the counterterm of Eq. 33:

$$\begin{aligned}
X_{CT}^{(s)} &= X_{CT}^{(t)} = \left(\frac{4\pi}{\alpha_s(\mu_R)} \right) \left[\delta Z_b^V + \frac{\delta m_b}{m_b} + \delta_{CT} \right] \\
&= \frac{4}{3} \left[2 M_{\tilde{g}} Y_b I(M_{\tilde{b}_1}, M_{\tilde{b}_2}, M_{\tilde{g}}) + \sum_{i=1}^{2} \left(-(-1)^i 2 m_b s_{2\tilde{b}} B_0' + 2 m_b^2 B_1' \right) (0; M_{\tilde{g}}^2, M_{\tilde{b}_i}^2) \right]
\end{aligned} \tag{78}$$

Note that the counterterm contains no large $\tan\beta$ enhanced contribution.

Appendix C: Definitions

In this appendix we define the f unctions used in the expansions of the Passarino-Veltman integrals in the maximum and minimum mixing scenarios, where $R \equiv \frac{M_{\tilde{g}}}{M_S}$ in the maximal

mixing scenario, and $R_i \equiv \frac{M_{\tilde{b}_i}}{M_S}$ in the minimal mixing scenario:

$$
\begin{aligned}
f_1(R) &= \frac{2}{(1-R^2)^2}\left[1-R^2+R^2\log R^2\right] \\
f_2(R) &= \frac{3}{(1-R^2)^3}\left[1-R^4+2R^2\log R^2\right] \\
f_3(R) &= \frac{4}{(1-R^2)^4}\left[1+\frac{3}{2}R^2-3R^4+\frac{1}{2}R^6+3R^2\log R^2\right] \\
f_4(R) &= \frac{5}{(1-R^2)^5}\left[\frac{1}{2}-4R^2+4R^6-\frac{1}{2}R^8-6R^4\log R^2\right] \\
h_1(R_1,R_2,n) &= \left(\frac{R_1^2}{1-R_1^2}\right)^n\frac{\log R_1^2}{1-R_1^2}-\left(\frac{R_2^2}{1-R_2^2}\right)^n\frac{\log R_2^2}{1-R_2^2} \\
&\quad -\sum_{j=0}^{n}(-1)^j\frac{j+2}{2}\left\{\left(1-R_1^2\right)^{j-n}-\left(1-R_2^2\right)^{j-n}\right\} \\
h_2(R_1,R_2) &= \frac{R_1^2+R_2^2-2}{(1-R_1^2)(1-R_2^2)}+\frac{1}{R_1^2-R_2^2}\left[\frac{R_1^2+R_2^2-2R_1^4}{(1-R_1^2)^2}\log R_1^2\right. \\
&\quad \left.-\frac{R_1^2+R_2^2-2R_2^4}{(1-R_2^2)^2}\log R_2^2\right].
\end{aligned}
\tag{79}
$$

Further,

$$
\begin{aligned}
f_i'(R) &\equiv \left.\frac{\mathrm{d}f_i(x)}{\mathrm{d}x^2}\right|_{x=R} \\
f_i^{-1}(R) &\equiv \frac{f_i(1/R)}{R^2} \\
\hat{f}_i(R) &\equiv \left.\frac{1}{R^4}\frac{\mathrm{d}f_i(x)}{\mathrm{d}x^2}\right|_{x=1/R}.
\end{aligned}
\tag{80}
$$

---

[1] A. Djouadi (2005), hep-ph/0503173.

[2] J. F. Gunion, H. E. Haber, G. L. Kane, and S. Dawson, *THE HIGGS HUNTER'S GUIDE* (Addison Wesley (Menlo Park), 1990).

[3] M. S. Carena and H. E. Haber, Prog. Part. Nucl. Phys. **50**, 63 (2003), hep-ph/0208209.

[4] D. Benjamin et al. (Tevatron New Phenomena and Higgs Working Group) (2010), 1003.3363.

[5] S. Chatrchyan et al. (CMS) (2011), 1104.1619.

[6] G. Aad et al. (The ATLAS) (2009), 0901.0512.

[7] G. L. Bayatian et al. (CMS), J. Phys. **G34**, 995 (2007).

[8] S. Dawson, C. B. Jackson, L. Reina, and D. Wackeroth, Phys. Rev. Lett. **94**, 031802 (2005), hep-ph/0408077.

[9] S. Dawson, C. B. Jackson, L. Reina, and D. Wackeroth, Mod. Phys. Lett. **A21**, 89 (2006), hep-ph/0508293.

[10] M. S. Carena, A. Menon, and C. E. M. Wagner, Phys. Rev. **D76**, 035004 (2007), arXiv:0704.1143 [hep-ph].

[11] J. Campbell et al. (2004), hep-ph/0405302.

[12] S. Dittmaier, M. Kramer, and M. Spira, Phys. Rev. **D70**, 074010 (2004), hep-ph/0309204.

[13] M. S. Carena, S. Mrenna, and C. E. M. Wagner, Phys. Rev. **D60**, 075010 (1999), hep-ph/9808312.

[14] S. Dawson, C. B. Jackson, L. Reina, and D. Wackeroth, Phys. Rev. **D69**, 074027 (2004), hep-ph/0311067.

[15] F. Maltoni, Z. Sullivan, and S. Willenbrock, Phys. Rev. **D67**, 093005 (2003), hep-ph/0301033.

[16] F. Maltoni, T. McElmurry, and S. Willenbrock, Phys. Rev. **D72**, 074024 (2005), hep-ph/0505014.

[17] D. Dicus, T. Stelzer, Z. Sullivan, and S. Willenbrock, Phys. Rev. **D59**, 094016 (1999), hep-ph/9811492.

[18] J. Campbell, R. K. Ellis, F. Maltoni, and S. Willenbrock, Phys. Rev. **D67**, 095002 (2003), hep-ph/0204093.

[19] S. Dittmaier et al. (LHC Higgs Cross Section Working Group) (2011), 1101.0593.

[20] B. Field, L. Reina, and C. B. Jackson, Phys. Rev. **D76**, 074008 (2007), 0705.0035.

[21] S. Dawson and P. Jaiswal, Phys. Rev. **D81**, 073008 (2010), 1002.2672.

[22] M. Beccaria et al., Phys. Rev. **D82**, 093018 (2010), 1005.0759.

[23] S. Dawson and C. B. Jackson, Phys. Rev. **D77**, 015019 (2008), 0709.4519.

[24] A. Dabelstein, Nucl. Phys. **B456**, 25 (1995), hep-ph/9503443.

[25] L. J. Hall, R. Rattazzi, and U. Sarid, Phys. Rev. **D50**, 7048 (1994), hep-ph/9306309.

[26] M. S. Carena, D. Garcia, U. Nierste, and C. E. M. Wagner, Nucl. Phys. **B577**, 88 (2000), hep-ph/9912516.

[27] J. Guasch, P. Hafliger, and M. Spira, Phys. Rev. **D68**, 115001 (2003), hep-ph/0305101.

[28] H. E. Haber et al., Phys. Rev. **D63**, 055004 (2001), hep-ph/0007006.

[29] R. V. Harlander and W. B. Kilgore, Phys. Rev. **D68**, 013001 (2003), hep-ph/0304035.

[30] S. Heinemeyer, W. Hollik, H. Rzehak, and G. Weiglein, Eur. Phys. J. **C39**, 465 (2005), hep-ph/0411114.

[31] A. Brignole, G. Degrassi, P. Slavich, and F. Zwirner, Nucl. Phys. **B643**, 79 (2002), hep-ph/0206101.

[32] D. Noth and M. Spira (2010), 1001.1935.

[33] D. Noth and M. Spira, Phys. Rev. Lett. **101**, 181801 (2008), 0808.0087.

[34] S. Heinemeyer, W. Hollik, and G. Weiglein, Comput. Phys. Commun. **124**, 76 (2000), hep-ph/9812320.

[35] G. Degrassi, S. Heinemeyer, W. Hollik, P. Slavich, and G. Weiglein, Eur. Phys. J. **C28**, 133 (2003), hep-ph/0212020.

[36] S. Heinemeyer, W. Hollik, and G. Weiglein, Eur. Phys. J. **C9**, 343 (1999), hep-ph/9812472.

[37] S. Dittmaier, M. Kramer, A. Muck, and T. Schluter, JHEP **03**, 114 (2007), hep-ph/0611353.

[38] M. S. Carena, M. Olechowski, S. Pokorski, and C. E. M. Wagner, Nucl. Phys. **B426**, 269 (1994), hep-ph/9402253.

[39] S. Dittmaier, M. Kramer, M. Spira, and M. Walser (2009), 0906.2648.

[40] E. L. Berger, T. Han, J. Jiang, and T. Plehn, Phys. Rev. **D71**, 115012 (2005), hep-ph/0312286.

[41] L. Hofer, U. Nierste, and D. Scherer, JHEP **10**, 081 (2009), 0907.5408.

[42] E. Accomando, G. Chachamis, F. Fugel, M. Spira, and M. Walser (2011), 1103.4283.

[43] S. Berge, W. Hollik, W. M. Mosle, and D. Wackeroth, Phys. Rev. **D76**, 034016 (2007), hep-ph/0703016.

[44] P. Nason, S. Dawson, and R. K. Ellis, Nucl. Phys. **B303**, 607 (1988).

[45] J. F. Gunion, H. E. Haber, and M. Sher, Nucl. Phys. **B306**, 1 (1988).

[46] P. M. Nadolsky et al., Phys. Rev. **D78**, 013004 (2008), 0802.0007.

[47] A. D. Martin, W. J. Stirling, R. S. Thorne, and G. Watt, Eur. Phys. J. **C63**, 189 (2009), 0901.0002.